Research Article

Do selectivity filter carbonyls in K$^+$ channels flip away from the pore? Two-dimensional infrared spectroscopy study

Nikhil Maroli [a], Matthew J. Ryan [b], Martin T. Zanni [b,*], Alexei A. Kananenka [a,*]

[a] Department of Physics and Astronomy, University of Delaware, Newark, DE 19716, USA
[b] Department of Chemistry, University of Wisconsin-Madison, Madison, WI 53706, USA

ARTICLE INFO

ABSTRACT

Molecular dynamics simulations revealed that the carbonyls of the Val residue in the conserved selectivity filter sequence TVGTG of potassium ion channels can flip away from the pore to form hydrogen bonds with the network of water molecules residing behind the selectivity filter. Such a configuration has been proposed to be relevant for C-type inactivation. Experimentally, X-ray crystallography of the KcsA channel admits the possibility that the Val carbonyls can flip, but it cannot decisively confirm the existence of such a configuration. In this study, we combined molecular dynamics simulations and line shape theory to design two-dimensional infrared spectroscopy experiments that can corroborate the existence of the selectivity filter configuration with flipped Val carbonyls. This ability to distinguish between flipped and unflipped carbonyls is based on the varying strength of the electric field inside and outside the pore, which is directly linked to carbonyl stretching frequencies that can be resolved using infrared spectroscopy.

Introduction

Potassium (K$^+$) ion channels are transmembrane proteins that are present in all cell types including neurons, muscle cells, and other tissues. KcsA, a prokaryotic pH-activated K$^+$ channel from *Streptomyces lividans*, was the first K$^+$ channel whose high-resolution crystal structure was determined (Doyle et al., 1998). The structure of the KcsA channel is formed from four identical subunits, each containing three α-helices located symmetrically around the central pore through which K$^+$ ions and water molecules pass (Alcayaga et al., 1989). K$^+$ ion flux in the KcsA channel is characterized by high transport rates (1 ion per 10 ns) and superb selectivity (Na$^+$:K$^+$=1:1000) (Littleton and Ganetzky, 2000; LeMasurier et al., 2001). KcsA serves as an important prototypical model to study K$^+$ channels because of its structural and functional similarity to eukaryotic K$^+$ channels (LeMasurier et al., 2001; MacKinnon et al., 1998; Cordero-Morales et al., 2006). Thus, elucidating the structure and function of the KcsA channel is pivotal for understanding a large class of biologically important ion channels.

The selectivity filter of the KcsA channel is the narrowest part of the pore and is the most rigid part of the protein (Fig. 1A) (Bernèche and Roux, 2000). It is a key determinant of the ion permeation, selectivity, and gating (Cordero-Morales et al., 2006; Demo and Yellen, 1992; Swenson and Armstrong, 1981). The selectivity filter is only 12 Å long, and it is located near the extracellular side of the channel. Backbone carbonyl groups of the conserved sequence T75-V76-G77-Y78-G79 form the selectivity filter. The carbonyl groups of this sequence point toward the center of the pore forming a set of octahedral cages of oxygens called binding sites. There are four binding sites denoted as S1, S2, S3, and S4, from extracellular to intracellular. S1, S2, and S3 sites are formed by the eight backbone carbonyls of the selectivity filter sequence. S4 site is composed by the four carbonyls and four hydroxyl groups of the T75 residue.

X-ray crystallography has provided the essential structural information about the KcsA channel, K$^+$ ions, and the structural water near the protein (Doyle et al., 1998; Cordero-Morales et al., 2006; Cuello et al., 2010; Zhou et al., 2001; Cuello et al., 2017; Valiyaveetil et al., 2006). However, X-ray experiments are inherently limited to static structures and cannot provide transient structures arising during the gating processes: activation, C-type inactivation, deactivation, and recovery from C-type inactivation. Additionally, only crystal structures of presumed open inactivated and closed conductive configurations of the KcsA channel have been determined so far. Despite improvements in the resolution of the X-ray technique, some details of the static KcsA structure remain uncertain.

---

* Corresponding authors.
E-mail addresses: zanni@chem.wisc.edu (M.T. Zanni), akanane@udel.edu (A.A. Kananenka).

One such structural detail that has not been experimentally tested is the conformational state of the selectivity filter, in which the V76 backbone carbonyl of one of the four subunits flips away from the pore instead of pointing toward the pore (Bernèche and Roux, 2000; Cuello et al., 2017). We will refer to this conformational state of the selectivity filter as "V76-flip" configuration. Experimentally, crystallographic *B*-factors of V76 carbonyls and the neighboring atoms in the KcsA structure are similar (Doyle et al., 1998; Cordero-Morales et al., 2006; Cuello et al., 2017).

Bernèche and Roux first observed a V76-flip configuration in molecular dynamics simulations of the KcsA channel (Bernèche and Roux, 2000; Bernèche and Roux, 2005). In this conformation, the NH group of the G77 residue forms a hydrogen bond with the water molecule located at the S2 site when V76 carbonyl rotates away from the pore. The lifetime of the V76-flip configuration was estimated to be on the order of milliseconds before V76 carbonyl flips back into the pore (Bernèche and Roux, 2005). Since the original observation, subsequent molecular dynamics simulations of the KcsA and other K^+ channels have also reported the V76-flipped configuration (Bernèche and Roux, 2005; Fowler et al., 2013; Domene and Sansom, 2003; Capener et al., 2003; Furini and Domene, 2020; Brennecke and De Groot, 2018; Fowler et al., 2008; Mendez-Otalvaro et al., 2004). According to molecular dynamics simulations, the V76-flip configuration has a pronounced impact on ion function. Flipping of V76 carbonyls bears an unconquerable energetic barrier for the ion movement along the selectivity filter (Cuello et al., 2010). This flip configuration was found to play an important role in the stability and ion selectivity under low-potassium conditions (Domene and Furini, 2009). V76 carbonyl flipping was proposed to be a key step in C-type inactivation, a slow process by which the channel enters a nonconductive conformation (Cuello et al., 2010; Bernèche and Roux, 2005; Furini and Domene, 2020; Li et al., 2018; Gibor et al., 2007). The flipped V76 carbonyl is hydrogen-bonded to a water molecule participating in the network of crystallographic water molecules located behind the selectivity filter in the so-called "inactivation cavity" (Cuello et al., 2010; Cuello et al., 2017).

Interestingly, the V76-flip configuration has been observed only for certain ion and water configurations in the selectivity filter, those in which K^+ ions alternate with water. The two relevant configurations are shown in Fig. 1C and will be denoted as [W,S2,W,S4] and [S1,W,S3,W].

These configurations are descriptive of the commonly accepted ion transport mechanism called "soft" knock-on (or simply soft-knock) (Zhou et al., 2001; Fowler et al., 2013; Morais-Cabral et al., 2001; Hodgkin and Keynes, 1955; Zhou and MacKinnon, 2003; Tilegenova et al., 2019; Iwamoto and Oiki, 2011; Rauh et al., 2018; Bernèche and Roux, 2001; Bernèche and Roux, 2003; Åqvist and Luzhkov, 2000; Berneche and Roux, 2000; Shrivastava and Sansom, 2000; Guidoni et al., 2000; Khalili-Araghi et al., 2006; Jensen et al., 2013; Allen et al., 1999; Furini and Domene, 2009; Heer et al., 2017). According to molecular dynamics simulations, the fraction of V76-flip carbonyls among the soft-knock configurations in the KcsA channel could reach *ca.* 30 % (Fowler et al., 2013). In contrast, the V76-flip configuration was not observed in the simulations with two K^+ ions simultaneously occupying the adjacent sites S2 and S3 in the selectivity filter or any other configuration representative of the "hard" knock-on (hard-knock) model (Bernèche and Roux, 2000; Furini and Domene, 2020; Jensen et al., 2013; Furini and Domene, 2009; Köpfer et al., 2014; Langan et al., 2018; Boiteux et al., 2020; Öster et al., 2019; Borcik et al., 2020; Eichmann et al., 2019; Kopec et al., 2018; Kopec et al., 2019; Schewe et al., 2016; Domene et al., 2021; Lam and de Groot, 2023).

Molecular dynamics simulations provide the detailed microscopic insight into the structure and dynamics of ion channels. However, care must be taken to ensure that the results are interpreted meaningfully. Molecular dynamics simulations of ion channels with different force fields have been shown to give rather divergent results (Furini and Domene, 2020; Fowler et al., 2008). Due to their relatively low computational cost, simulations of ion channels often employ classical nonpolarizable force fields that do not describe polarization and charge-transfer effects in protein-K^+ interactions inside the selectivity filter. These effects, however, could be significant and may even play a role in high ion selectivity of the KcsA channel (Furini and Domene, 2020; Guidoni and Carloni, 2002; Klesse et al., 2020; Kraszewski et al., 2009; Compoint et al., 2004; Bucher et al., 2006; Huetz et al., 2006; Noskov and Roux, 2006). One can approximately account for these effects by using the partial charges of K^+ ions instead of "+1" (a.u.) charge usually taken in molecular dynamics simulations. The partial charges could, e. g., be derived from the electrostatic potential (Kraszewski et al., 2009; Huetz et al., 2006; Chirlian and Francl, 1987; Ritchie and Bachrach, 1987; Breneman and Wiberg, 1990).
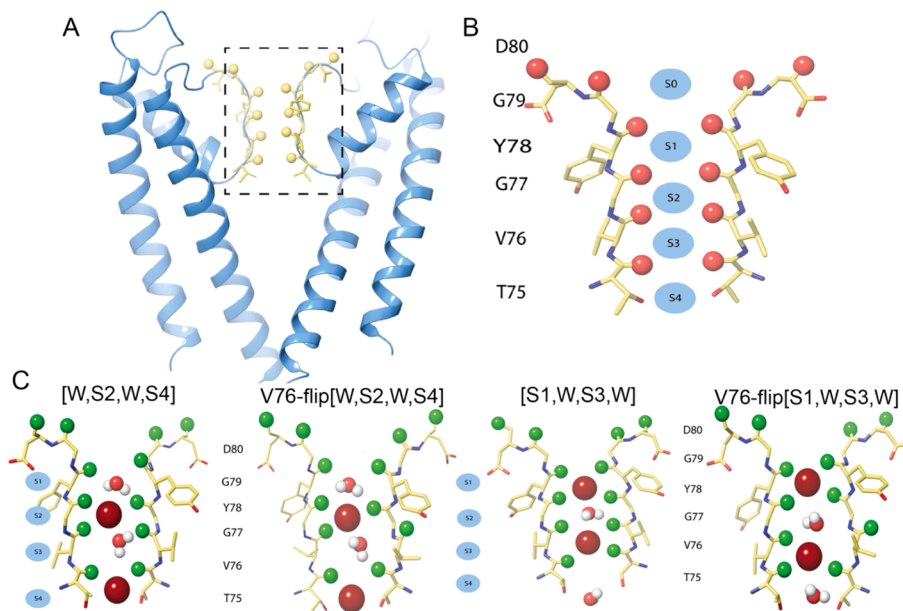

Fig. 1. A. Schematic illustration of the pore domain of the KcsA channel with closed intracellular gate and a conductive selectivity filter. Only two out of four protein chains are shown for clarity. Selectivity filter residues are colored yellow, with the carbonyls forming binding sites shown as yellow spheres. B. Selectivity filter residues and binding sites. The carbonyls shown as red spheres. C. Two configurations of the selectivity filter shown with V76 carbonyl flipped and unflipped.

Mixed quantum–classical vibrational line shape theory connects structures from molecular dynamics simulations to experimental observables and can be used to validate molecular dynamics force fields and simulation protocols. Two-dimensional infrared spectroscopy (2D IR) is a structure-sensitive technique that measures molecular vibrations (Hamm and Zanni, 2011; Petti et al., 2018; Ghosh et al., 2017). Specifically, amide I vibrations (predominantly the carbonyl stretch) are very sensitive reporters of the local chemical environment of the peptide group (Baiz et al., 2020; Reppert and Tokmakoff, 2016). Kratochvil *et al.* (Kratochvil et al., 2016) measured 2D IR spectrum of the KcsA channel in the amide I region. Their goal was not to study the elusive V76-flip state, but to elucidate K$^+$ ions and water configurations inside the selectivity filter. They isotope-labeled V76, G77, and G79 carbonyls with ^{13}C^{18}O. Such isotope-labeling redshifts the amide I frequency by 66 cm^{-1}, spectroscopically isolating it from the other amide I vibrations in the protein enabling selective probing of specific binding sites in the selectivity filter. With the help of molecular dynamics simulations and line shape modeling, they concluded that the 2D IR spectrum of the three configurations [W,S2,W,S4], [S1,W,S3,W], and V76-flip[S1,W,S3,W] taken at 3:3:4 ratio best fits the experimental 2D IR spectrum for the triple isotope-labeled selectivity filter (Fig. 2). Recently, some of the present authors measured 2D IR spectra of the KcsA channel with V76

and G77 residues ^{13}C^{18}O isotope-labeled in two separate experiments (Ryan et al., 2023). They too used simulations to interpret the spectra and reported that the best agreement between experiment and simulations was achieved for [W,S2,W,S4]:[S1,W,S3,W] = 3:2 mixture. The absence of clear experimental evidence for the V76-flipped configuration precluded us from interpreting the spectra in terms of this configuration. However, while analyzing the simulated 2D IR spectra we made two important observations. First, we noted that flipping one V76 carbonyl group in a small fraction of [W,S2,W,S4] configurations still yields a 2D IR spectrum that is in a similarly good agreement with experiment as long as K$^+$ charges are taken to be "+1" (a.u.). This low-V76-flip mixture [W,S2,W,S4]:[S1,W,S3,W]:Val76-flip[W,S2,W,S4] = 5:4:1 will be referred to as "set1". Secondly, we observed that the experimental V76 and G77-labeled spectra can be well reproduced in a simulation of [S1,W,S3,W]:V76-flip[W,S2,W,S4]:V76-flip[S1,W,S3, W] = 4:3:3 mixture ("set2") with a set of scaled K$^+$ charges determined from *ab initio* calculations (Kraszewski et al., 2009). To summarize, the two sets of alternating ion-water configurations in the selectivity filter denoted as set1 and set2 containing 10 % and 60 % of V76-flipped configuration and calculated with +1 (a.u.) and scaled K$^+$ charges, respectively, could not be distinguished by single isotope labeled V76 and G77 and triple isotope labeled V76-G77-G79 2D IR experiments. We
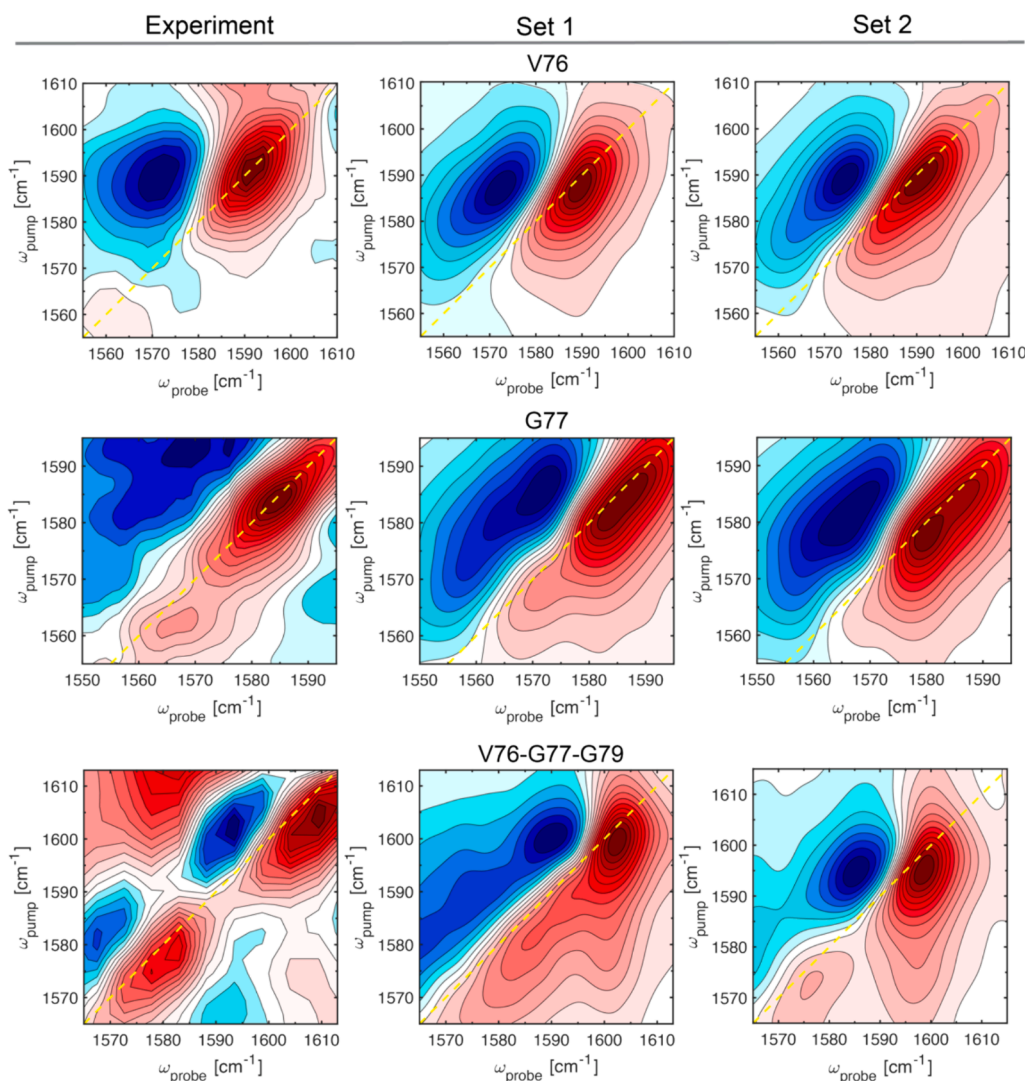

Fig. 2. Experimental (Kratochvil et al., 2016, Ryan et al., 2023) and simulated 2D IR spectra for V76, G77, and V76-G77-G79 isotope labeled selectivity filter of the KcsA channel. Simulated spectra are for the following configurations [W,S2,W,S4]:[S1,W,S3,W]:V76-flip[W,S2,W,S4] = 5:4:1 (set1) calculated with +1 (a.u.) charges for K$^+$ ions and [S1,W,S3,W]:V76-flip[W,S2,W,S4]:V76-flip[S1,W,S3,W] = 4:3:3 (set2) calculated with the scaled K$^+$ charges. See main text for details.

emphasize that 2D IR experiments described above were designed to decrypt ion/water configurations in the selectivity filter of the KcsA channel and not to test the existence of V76-flip configuration. Here, we computationally design a 2D IR experiment that shows the spectroscopic signatures of the V76-flip state and discriminates between set1 and set2 configurations.

The interior of the pore with K$^+$ ions and slow but dynamic water at S2 and S3 sites constitutes a noticeably different chemical environment for V76 carbonyls than the protein and structural waters residing behind the selectivity filter (Ryan et al., 2024). K$^+$ ions in the selectivity filter shift amide I frequencies by as much as 100 cm^{-1} compared to gas phase, while protein and water cause smaller frequency shifts (Ryan et al., 2024). Therefore, one might expect that amide I vibrational frequencies for the V76 residue pointing toward and away the pore can be different enough to be resolved in a purposefully designed 2D IR experiment. One triple-labeled and two single-labeled experiments performed thus far have explored only three out of fifteen possibilities for isotope-labeling of the five selectivity filter residues. In this study we exhaustively simulated all possible single, double, and triple isotope-labeled 2D IR spectra of the KcsA channel and propose an experiment that can decisively prove or invalidate the V76-flip state. Performing all 15 isotope-label experiments including synthesis, assembly of the KcsA, and 2D IR measurements is a daunting task. In contrast, 2D IR spectra can now be straightforwardly simulated with sufficient accuracy. Taking previous 2D IR experiments into account effectively reduces the task to finding the set of isotope labels whose 2D IR spectrum for set1 would be sufficiently different from that of set2.

Methods

Molecular dynamics simulations

Molecular dynamics trajectories used in this study were taken from Kratochvil et al (Kratochvil et al., 2016). The crystallographic structure of the KcsA channel (pdb:1K4C; 2.0 Å resolution (Zhou et al., 2001)) using residues Ser22 to His124 was embedded in a 71 Å x 71 Å bilayer consisting of 117 dipalmitoyl-phosphatidylcholine (DPPC) lipid molecules. The system was solvated with water molecules. K$^+$ and Cl$^-$ ions were added to the bulk solution to neutralize the charge of the system and establish a KCl concentration of 500 mM. K$^+$ ions and water molecules were placed at the designated binding sites to create [W,S2,W,S4] and [S1,W,S3,W] configurations. A polarizable force field based on classical Drude polarizable models was used for the KcsA and DPPC (Lopes et al., 2013; Chowdhary et al., 2013). This force field explicitly accounts for electronic polarizability by including the flexible point charge particles from heavy atoms (Lopes et al., 2013; Chowdhary et al., 2013). Polarizable force fields were used because they provide a better description of ion-protein interactions (Klesse et al., 2020; Li et al., 2015; Jing et al., 2019). K$^+$ and Cl$^-$ parameters that represent improved ion-protein interactions were taken from Li et al. (Li et al., 2015). SWM4 water model was used (Lamoureux et al., 2006). For each ion configuration the simulation system was first equilibrated at constant pressure of 1 atm and temperature 298.15 K (NPT). This was followed by a production simulation at constant volume and temperature 298.15 K (NVT). The temperature of the system was maintained by coupling to a Langevin thermostat, with temperatures of the Drude particles maintained at 1 K. Electrostatic interactions were treated using the Particle Mesh Ewald (PME) method (Petersen, 1995). Electrostatic and van der Waals forces were smoothly truncated with the cut-off of 12 Å. A 5 kcal/mol harmonic restraints were applied to the protein C$_\alpha$ atoms, excluding those of the selectivity filter. The selectivity filter residues (74 to 79) were constrained using a spring constant of 2000 kJ/mol/nm^2. The coordinates of the K$^+$ ions in each binding site of the selectivity filter were constrained with flat bottom potentials. Water molecules were not constrained. Approximately 100 configurations were generated for each simulation system at intervals of at least 50 ps. NAMD2.10 package was

employed in simulations using Drude polarizable force field (Phillips et al., 2005). Each configuration is then employed as the starting structure for further MD simulations for 2D IR spectroscopy calculations. In these simulations GROMOS96 53a6 force field and SPC water model were used (Scott et al., 1999; Oostenbrink et al., 2004). This combination of force fields was used because it was previously used to develop electrostatic maps for calculating 2D IR spectra. Systems were first minimized using the steepest descent algorithm. Then a 20-ps long trajectory was generated by performing MD simulations at NVT ensemble with a 2 fs integration time step. The coordinates of all atoms were saved every 20 fs and used in spectroscopy calculations as described below. GROMACS 5.0.4 package was used in GROMOS96 simulations (Van Der Spoel et al., 2005).

Calculation of 2D IR spectra

2D IR spectra were calculated using a mixed quantum–classical approach based on vibrational frequency and coupling maps (Baiz et al., 2020; Wang et al., 2011; Wang et al., 2011; Liang and Jansen, 2012). The amide I frequencies were calculated using electrostatic frequency maps, developed by Wang *et al.,* (Wang et al., 2011) and nearest-neighbor (NN) frequency maps (la Cour Jansen et al., 2006). The former relate the frequency of the i th amide I chromophore ω_i (in cm^{-1}) to local electric fields: $\omega_i = 1684 + 7729 E_{C_i} - 3576 E_{N_i}$, where E_{C_i} and E_{N_i} are the electric fields (in atomic units) in the C = O bond direction on the amide C and N atoms. These fields are due to peptide atoms that are more than 3 covalent bonds away from the peptide group and all other atoms including water, K$^+$ ions, and lipids within a cut-off of 20 Å. Electric fields were calculated from the point charges from GROMOS96 53a6 and SPC force fields. This combination of force fields was chosen because it was used to parametrize the electrostatic frequency map of Wang *et al.* (Wang et al., 2011). NN frequency maps account for the frequency shifts due to covalent through-bond effects from the nearest-neighbor amide groups. These frequency shifts depend on Ramachandran angles as explained in la Cour Jansen et al., 2006. The remaining contribution to amide I frequency is the frequency shift due to $^{13}C^{18}O$ isotope label which was set to -66 cm^{-1}. The vibrational anharmonicity was set to 14 cm^{-1} as determined experimentally in Mukherjee et al., 2006. The lifetime of the first excited state of an amide I chromophore was assumed to be independent of the residue and was set to 600 fs (Mukherjee et al., 2004). In 2D IR calculations vibrational couplings between nearest-neighbor amide I chromophores were treated using nearest-neighbor coupling maps (la Cour Jansen et al., 2006). Longer-range couplings were treated using the transition dipole coupling scheme (Wang et al., 2011; Torii and Tasumi, 1998). Amide I transition dipoles were calculated using the model of Torii and Tasumi. Frequencies, couplings, and transition dipole moments were calculated using MultiSpec program (https://github.com/kananenka-group/MultiSpec). 2D IR spectra in ZZZZ polarization were calculated using NISE program (Liang and Jansen, 2012). 2D IR spectra were calculated for two sets of K$^+$ charges: +1 (a.u.) and partial charges from Kraszewski et al., 2009. discussed below.

The accuracy of this approach was assessed by Carr *et al.* (Carr et al., 2014) and later by Cunha *et al.* (Cunha et al., 2016). The former used experimental gas-phase IR spectra of Phe-(Ala)$_5$-Lys-H$^+$ peptide as a reference. The average unsigned error for the vibrational frequencies was less than 4 cm^{-1}, and the largest error was 11 cm^{-1}. The assessment of Cunha *et al.* (Cunha et al., 2016) was based on 2D IR spectra of lysozyme, ribonuclease A, and concanavalin A in water. For the Gromos96 54a7 (Oostenbrink et al., 2004) and SPC (Berendsen et al., 1981) force fields and spectroscopic maps used here (Wang et al., 2011) the average frequency error was 4.8 cm^{-1} and the maximum error was 10.3 cm^{-1}, in agreement with earlier results of Carr *et al.* (Carr et al., 2014).

Scaling of ion charges is often used to approximately account for polarization and charge-transfer effects between the ions and backbone carbonyls which influence the binding and, in turn, affect the

conductance and selectivity of a channel (Kraszewski et al., 2009; Compoint et al., 2004; Bucher et al., 2006; Huetz et al., 2006). Different methods can be used for evaluating partial K^+ charges (Breneman and Wiberg, 1990; Chirlian and Francl, 1987; Compoint et al., 2004; Huetz et al., 2006; Kraszewski et al., 2009; Ritchie and Bachrach, 1987). For example, Huetz *et al.* (Compoint et al., 2004; Huetz et al., 2006) calculated Merz-Kollman (MK) (Besler et al., 1990; Singh and Kollman, 1984) and Hinsen-Roux (HR) (Hinsen and Roux, 1997) charges for [W,S2,W, S4] configuration using Hartree-Fock (HF) method. In both methods the charges were fitted to best reproduce HF ESP. The resulting K^+ charges range from 0.76 to 0.88 (a.u.) for K^+ in S2 to 0.68–0.88 for K^+ in S4 (Compoint et al., 2004; Huetz et al., 2006) Later Kraszewski *et al.* (Kraszewski et al., 2009) determined the partial charges for all four S1-S4 sites by using the MK scheme, again, based on HF ESP. The final K^+ charges are: +1.0 for S1, +0.83 (S2), +0.91 (S3), and + 0.85 (S4) (all in a.u.). The partial charges are sensitive to the method used to obtain them. Likewise, they will be sensitive to the geometry and the local environment of the selectivity filter. In this study, we use the charges from Kraszewski et al., 2009 because they provide a complete set of S1-S4 charges and they have been used in previous 2D IR simulations (Kratochvil et al., 2016; Ryan et al., 2023; Strong et al., 2020). Investigating the effect of the partial K^+ and protein charges on 2D IR spectra is outside of the scope of the present study. A potentially better and more accurate approach would entail using polarizable force fields (Klesse et al., 2020; Li et al., 2015; Warshel et al., 2007) which we plan to address in future publications.

Calculation of center line slope

Center line slope (CLS) was used as one of the criteria for distinguishing 2D IR spectra. CLS was introduced by Kwak *et al.* (Kwak et al., 2007, 2008) as a measure of the tilt of the diagonally elongated 2D IR lineshape. Mathematically, the CLS can be expressed as $CLS = d\omega_{probe,max}/d\omega_{pump}$. It can be computed by taking slices through the 2D spectrum parallel to the detection frequency axis (ω_{probe}). Each slice is a one-dimensional spectrum. The slope of the line $\omega_{probe,max}(\omega_{pump})$ connecting the frequencies of the maxima of the sliced spectra is the CLS. $\omega_{probe,max}$ can be taken directly from the data as the frequency with the maximum calculated signal as it is done here. Alternatively, each pump slice can be fitted to a simple function, such as Gaussian, and then $\omega_{probe,max}$ can be determined from the fit's maximum. CLS is a useful measure of 2D IR line shape inhomogeneity. A perfectly homogeneous lineshape is characterized by the round 2D line shape with the slope being 0. A perfectly inhomogeneous lineshape is completely extended along the diagonal and has a slope of 1.

Results and discussion

We consider two 2D IR spectra to be sufficiently different if they satisfy one or more of the following criteria: *a)* different number of distinct peaks, *b)* peak frequency difference is larger than the uncertainty due to spectroscopic maps which, as discussed above, is *ca.* 10 cm^{-1}, *c)* the CLS of the two peaks must be sufficiently different. For example, when one spectrum is close to the homogeneous limit (CLS < 0.5) while the other spectrum is close to the inhomogeneous limit (CLS > 0.5). Simultaneous fulfillment of all three criteria is not required, and as will be demonstrated below, is not possible for the problem under study.

Table 1 summarizes the results for all fifteen possible 2D IR spectra. According to Table 1 the four most distinctive experiments are all with triple labeled residues: *i)* T75-V76-Y78, *ii)* T75-G77-Y78, *iii)* T75-G77-G79, and *iv)* T75-V76-G77. The two important observations are: all four experiments involve isotope labeling of the T75 residue and may not involve labeling the V76 residue even though it is the flip of the V76 carbonyl that is being probed.

Table 1

Peak frequencies, frequency differences, and center line slopes of simulated 2D IR spectra for the two sets of configurations: [W,S2,W,S4]:[S1,W,S3,W]:V76-flip [W,S2,W,S4] = 5:4:1 (set1) calculated with +1 (a.u.) charges of K^+ ions and [S1, W,S3,W]:V76-flip[W,S2,W,S4]:V76-flip[S1,W,S3,W] = 4:3:3 (set2) calculated with the scaled K^+ charges.

Isotope-labeled residues	Peak(s) frequency (cm^{-1})		Difference (cm^{-1})	Center Line Slope(s)	
	Set 1	Set 2		Set 1	Set 2
T75	1596	1606	10	0.50	0.67
		1587			0.41
V76	1589	1587	2	0.76	0.72
G77	1577	1584	7	0.87	0.84
Y78	1577	1577	0	0.54	0.73
G79	1576	1573	3	0.50	0.44
T75-V76	1601	1609	8	0.68	0.55
		1587			0.41
T75-G77	1596	1605	9	0.54	0.74
		1586			0.68
T75-Y78	1596	1606	10	0.54	0.67
	1577	1575	2	0.41	0.52
T75-G79	1596	1606	10	0.48	0.71
	1575	1573	2	0.32	0.62
V76-G77	1595	1600	4	0.62	0.53
V76-Y78	1585	1587	2	0.84	0.72
V76-G79	1587	1587	0	0.95	0.80
G77-Y78	1583	1584	1	0.89	0.76
G77-G79	1578	1581	3	0.83	0.87
Y78-G79	1578	1578	0	0.74	0.61
G77-Y78-G79	1582	1581	1	0.78	0.94
V76-Y78-G79	1584	1585	1	0.94	0.85
V76-G77-G79	1595	1600	5	0.60	0.58
	1573			0.36	
V76-G77-Y78	1596	1600	4	0.62	0.53
	1570			0.32	
T75-Y78-G79	1600	1606	6	0.55	0.63
	1577	1574	3	0.60	0.72
T75-G77-G79	1594	1607	13	0.48	0.77
		1580		0.95	0.65
T75-G77-Y78	1595	1607	12	0.59	0.77
		1590			0.70
T75-V76-G79	1601	1609	8	0.65	0.55
		1590			0.60
T75-V76-Y78	1601	1609	8	0.73	0.60
		1585			0.53
T75-V76-G77	1602	1611	9	0.51	0.52
		1590			0.47

Simulated 2D IR spectra for *i)-iv)* experiments and both sets of configurations are shown in Fig. 3. All 2D IR spectra, except for T75-V76-G77 set1 spectrum, have two peaks with varying intensity ratios. The two largest peak frequency differences for the higher-frequency peak were observed for T75-G77-G79 (13 cm^{-1}) and T75-G77-Y78 (12 cm^{-1}). Both can be resolved confidently with the presently used simulation methods. T75-V76-G77 and T75-V76-Y78 2D IR spectra have smaller difference between the high-frequency peaks of the two sets: 9 cm^{-1} and 8 cm^{-1}, respectively. However, the intensity ratio between the higher- and lower-frequency peaks in the T75-V76-Y78 spectrum is larger than in the T75-G77-G79 and T75-G77-Y78 spectra. Importantly, the T75-V76-G77 spectrum has only one clear peak. The CLS of the high-frequency peaks of T75-G77-G79 and T75-G77-Y78 2D IR spectra for the set1 indicate that these peaks are more inhomogeneously broadened than the high-frequency peaks of the set2 spectra. The CLS of the higher frequency peaks of T75-V76-G77 and T75-V76-Y78 are essentially the same for set1 and set2 spectra and are more homogeneous. We conclude that T75-G77-G79 and T75-G77-Y78 spectra satisfy the criteria b) and c) but not a). The T75-V76-Y78 spectra fulfill only criterion b). The T75-V76-G77 spectrum satisfy criterion a) and come only a few wavenumbers short to satisfying the criterion b). Because the latter is based on the worst-case scenario of the largest frequency error these peaks are likely resolvable, especially given a very good agreement between our
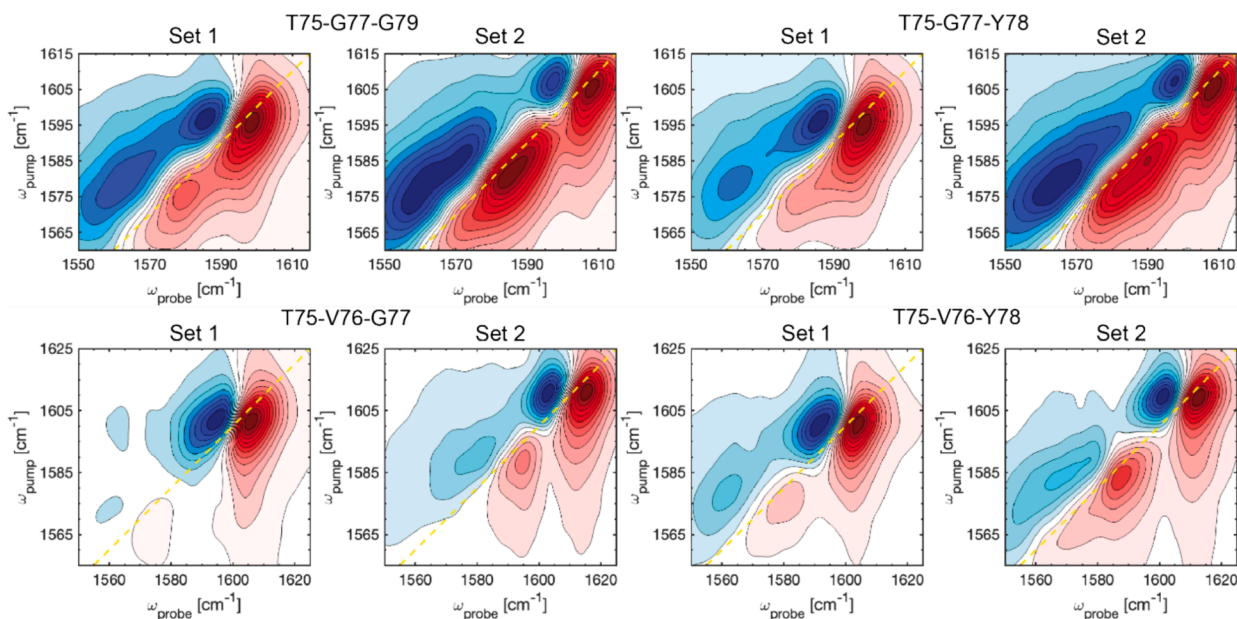
Fig. 3. 2D IR spectra of isotope labeled selectivity filter of the KcsA channel for the two sets of configurations [W,S2,W,S4]:[S1,W,S3,W]:V76-flip[W,S2,W,S4] = 5:4:1 (set1) calculated with +1 (a.u.) charges of K$^+$ ions and [S1,W,S3,W]:V76-flip[W,S2,W,S4]:V76-flip[S1,W,S3,W] = 4:3:3 (set2) calculated with the scaled K$^+$ charges.

previous simulations and experiments for the single-labeled KcsA selectivity filter (Ryan et al., 2023). Most importantly, 2D IR spectra of T75-V76-G77 labeling scheme of set1 has one peak, while in the case of set2 there are two peaks. Therefore, we conclude that the T75-V76-G77 experiment should distinguish between set1 and set2. T75-G77-Y78 experiment is a close second; both set1 and set2 2D IR spectra have two peaks with easily distinguishable intensity differences of the lower- and higher- frequency peaks separated by 8 cm^{-1}.

We now focus on 2D IR spectra of T75-V76-G77 isotope-labeled KcsA channel and analyze the contribution of each configuration. The corresponding spectra are shown in Fig. 4. Set1 comprises [W,S2,W,S4] and [S1,W,S3,W] configurations with the peaks at 1600 cm^{-1} and 1605 cm^{-1}, respectively. These two peaks add up with a 5:4 ratio to create the high-frequency peak at 1602 cm^{-1}. The V76-flip[W,S2,W,S4] spectrum has a single peak at 1595 cm^{-1}. Because this frequency is close to those of the other two configurations and the weight of this configuration is

only 10 %, this peak does not distinctively appear in the 2D IR spectrum of set1. Set2 comprises [S1,W,S3,W], V76-flip[W,S2,W,S4], and V76-flip[S1,W,S3,W] configurations and requires using scaled K$^+$ charges to achieve a good agreement with the existing 2D IR experiments. The corresponding 2D IR spectra are shown in the lower panel of Fig. 4. [S1,W,S3,W] and V76-flip[W,S2,W,S4] give peaks at 1611 cm^{-1}. The V76-flip[W,S2,W,S4] spectrum has another peak at 1590 cm^{-1}. 2D IR spectrum of V76-flip[S1,W,S3,W] configuration has only one inhomogeneously broadened peak centered at 1590 cm^{-1} as well. These two peaks add up with approximately the same weights to create a lower-frequency peak in the set2 spectrum centered at 1590 cm^{-1}.

Comparing the highest-frequency peaks in 2D IR spectra calculated with the scaled and unscaled K$^+$ charges, we note a frequency shift with the magnitude depending on the configuration: 15 cm^{-1} for [W,S2,W,S4] and V76-flip[W,S2,W,S4], 3 cm^{-1} for [S1,W,S3,W] and 5 cm^{-1} for V76-flip[S1,W,S3,W]. The shift is due to the reduction of the electric
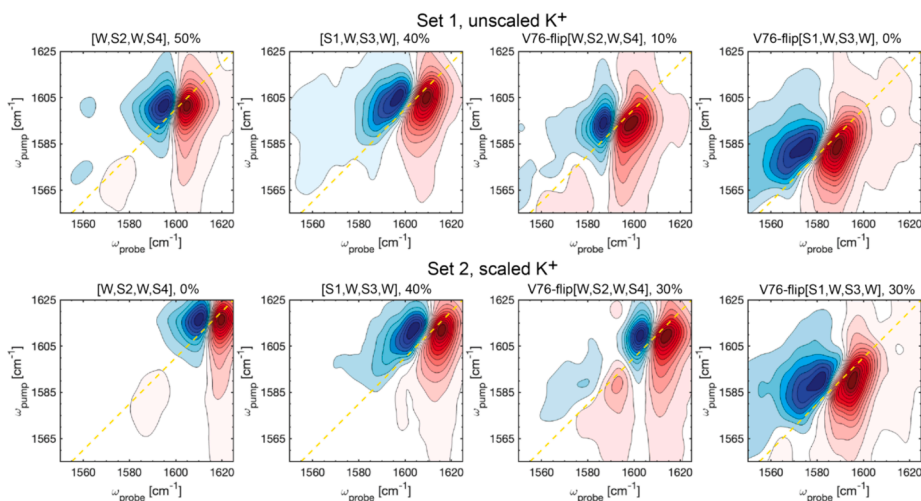

Fig. 4. 2D IR spectra of T75-V76-G77 isotope labeled selectivity filter of the KcsA channel for the four ion configurations that comprise the two sets of configurations considered in this work. The top panel shows the 2D IR spectra calculated by using +1 (a.u.) K$^+$ charges, the bottom panel shows the spectra calculated with the scaled K$^+$ charges.

field at the C and O atoms of the carbonyl group due to reduced K^+ charges. The frequency shift for (V76-flip)[S1,W,S3,W] compared to (V76-flip)[W,S2,W,S4] configurations is smaller because the charge reduction at the S3 site is smaller compared to that of S2 site and the electric field felt by the V76 carbonyls of the [S1,W,S3,W] configuration is weaker. The latter is because, as we showed previously (Ryan et al., 2024), the water molecule occupying the S2 binding site of the [S1,W,S3,W] configuration can reside near V76 carbonyls longer than the characteristic timescale of 2D IR experiments, making intermittent hydrogen bonds with them, and effectively screening the carbonyls from the field due to K^+ ions.

We now explain why T75-V76-G77 spectra are sensitive to the V76-flip configuration. In our V76-flip[W,S2,W,S4] and V76-flip[S1,W,S3, W] configurations, one V76 carbonyl is flipped away from the pore at all times while three others still point to the pore, in agreement with other molecular dynamics simulations (e.g., Furini and Domene, 2020). Because of different environments, flipped and unflipped V76 carbonyls are likely to have distinct spectral features. For $+1$ (a.u.) K^+ charges, the average vibrational frequencies of T75 and unflipped V76 carbonyls are 1593 cm^{-1} and 1587 cm^{-1}, respectively (Fig. 4). These vibrations are coupled, yielding the main peak that is inhomogeneously broadened and centered at 1595 cm^{-1}. Flipped V76 carbonyls and G77 carbonyls have the average frequencies of 1569 cm^{-1} and 1567 cm^{-1}, respectively. They are nearly 30 cm^{-1} red-shifted from the main peak. The coupling between them would create a doublet of peaks slightly below and above the two respective frequencies. Indeed, a weak feature near 1560–1575 cm^{-1} is present in the simulated spectrum but its intensity is tiny. Only 10 % of this, already weak, intensity contributes to the total T75-V76-G77 2D IR spectrum. This would make the V76-flip peak extremely hard to decisively discern experimentally.

In contrast, the 2D IR spectrum of the V76-flip[W,S2,W,S4] configuration with the scaled K^+ charges has two peaks. T75 carbonyls and unflipped V76 carbonyls have the average frequencies of 1608 cm^{-1} and 1607 cm^{-1}, respectively. Both contribute to the main peak at 1611 cm^{-1}. G77 carbonyl frequencies shift to 1582 cm^{-1} when K^+ charges are reduced. Flipped V76 carbonyls shift to 1580 cm^{-1}. Both contribute to the lower frequency peak at 1590 cm^{-1}. This peak, however, is only 20 cm^{-1} lower than the high-frequency peak and it is much more intense than the spectral feature due to G77 and V76-flipped carbonyls in the case of $+1$ (a.u.) K^+ charge. The larger intensity of the lower-frequency peak in this case is likely due to the larger extent of the vibrational exciton delocalization due to a stronger mixing between (T75,V76) and (V76-flip,G77) pairs of carbonyl frequencies which, in turn, is caused by the smaller frequency difference between them. Of course all four carbonyls are coupled, but the coupling within (T75,V76) and (V76-flip, G77) pairs is stronger than between the two pairs. When the scaled K^+ charges are used, the coupling between the pairs is stronger compared to the $+1e$ K^+ charges. Therefore, the basis for distinguishability between V76 flipped and unflipped configurations is twofold: *i)* a small fraction of V76-flip configuration in the case of set1 and *ii)* reduced K^+ charge leads to a smaller frequency difference between (T75,V76) and (V76-flip,G77) peaks and the larger intensity of the lower-frequency peak.

Conclusions

Selectivity filter carbonyls flipped away from the pore in K^+ channels were observed in molecular dynamics simulations, but conclusive experimental validation of such a configuration remains elusive. In this study, we used simulations to propose a 2D IR experiment that would shed light on this intriguing structural feature of K^+ channels. The proposed experiment would use triple isotope-labeled $^{13}C^{18}O$ carbonyls of T75, V76, and G77 selectivity filter residues. 2D IR spectra of the two mixtures of configurations containing high (60 %) and low (10 %) fractions of the V76 flipped carbonyls, which were indistinguishable in previous 2D IR experiments, can be resolved with the presented isotope-labeling scheme. The key to distinguishing the two configurations is the

vibrational frequency difference between flipped and unflipped carbonyls tuned by the charge of K^+ ions. This Article illustrates the power of 2D IR spectroscopy for providing structural details that are difficult to obtain with established biophysical structural techniques. A salient feature of 2D IR spectroscopy, illustrated here, is that amide I 2D IR spectra of proteins can now be routinely and accurately simulated using molecular dynamics and mixed quantum–classical line shape theory. This approach is an efficient means of testing hypothetical structures that can be used to interpret existing and design future experiments.

CRediT authorship contribution statement

Nikhil Maroli: Writing – review & editing, Formal analysis, Investigation. **Matthew J. Ryan:** Writing – review & editing, Formal analysis, Investigation. **Martin T. Zanni:** Writing – review & editing, Supervision, Resources, Methodology, Investigation, Funding acquisition, Formal analysis, Conceptualization. **Alexei A. Kananenka:** Writing – review & editing, Writing – original draft, Validation, Supervision, Software, Resources, Project administration, Methodology, Investigation, Funding acquisition, Formal analysis, Conceptualization.

Declaration of competing interest

M.T.Z. is a co-owner of PhaseTech Spectroscopy, which sells ultrafast pulse shapers and multidimensional spectrometers.

Data availability

Data will be made available on request.

References

Alcayaga, C., Cecchi, X., Alvarez, O., Latorre, R., 1989. Streaming potential measurements in Ca^{2+}-activated K^+ channels from skeletal and smooth muscle. Coupling of ion and water fluxes. Biophys. J. 55 (2), 367–371.

Allen, T.W., Kuyucak, S., Chung, S.-H., 1999. Molecular Dynamics Study of the KcsA Potassium Channel. Biophys. J. 77 (5), 2502–2516.

Åqvist, J., Luzhkov, V., 2000. Ion permeation mechanism of the potassium channel. Nature 404 (6780), 881–884.

Baiz, C.R., Błasiak, B., Bredenbeck, J., Cho, M., Choi, J.-H., Corcelli, S.A., Dijkstra, A.G., Feng, C.-J., Garrett-Roe, S., Ge, N.-H., et al., 2020. Vibrational Spectroscopic Map, Vibrational Spectroscopy, and Intermolecular Interaction. Chem. Rev. 120 (15), 7152–7218.

Berendsen, H.J.C., Postma, J.P.M., Van Gunsteren, W.F., Hermans, J., 1981. Interaction Models for Water in Relation to Protein Hydration. Springer, Netherlands, pp. 331–342.

Bernèche, S., Roux, B., 2003. A microscopic view of ion conduction through the K^+ channel. Proc. Natl. Acad. Sci. USA 100 (15), 8644–8648.

Berneche, S., Roux, B., 2000. Molecular dynamics of the KcsA K^+ channel in a bilayer membrane. Biophys. J. 78 (6), 2900–2917.

Bernèche, S., Roux, B., 2000. Molecular Dynamics of the KcsA K^+ Channel in a Bilayer Membrane. Biophys. J. 78 (6), 2900–2917.

Bernèche, S., Roux, B., 2001. Energetics of ion conduction through the K^+ channel. Nature 414 (6859), 73–77.

Bernèche, S., Roux, B., 2005. A Gate in the Selectivity Filter of Potassium Channels. Structure 13 (4), 591–600.

Besler, B.H., Merz Jr., K.M., Kollman, P.A., 1990. Atomic charges derived from semiempirical methods. J. Comput. Chem. 11 (4), 431–439.

Boiteux, C., Posson, D.J., Allen, T.W., Nimigean, C.M., 2020. Selectivity filter ion binding affinity determines inactivation in a potassium channel. Proc. Natl. Acad. Sci. U. S. A. 117 (47), 29968–29978.

Borcik, C.G., Versteeg, D.B., Amani, R., Yekefallah, M., Khan, N.H., Wylie, B.J., 2020. The lipid activation mechanism of a transmembrane potassium channel. J. Am. Chem. Soc. 142 (33), 14102–14116.

Breneman, C.M., Wiberg, K.B., 1990. Determining atom-centered monopoles from molecular electrostatic potentials. The need for high sampling density in formamide conformational analysis. J. Comput. Chem. 11 (3), 361–373.

Brennecke, J.T., De Groot, B.L., 2018. Mechanism of Mechanosensitive Gating of the TREK-2 Potassium Channel. Biophys. J. 114 (6), 1336–1343.

Bucher, D., Raugei, S., Guidoni, L., Dal Peraro, M., Rothlisberger, U., Carloni, P., Klein, M.L., 2006. Polarization effects and charge transfer in the KcsA potassium channel. Biophys. Chem. 124 (3), 292–301.

Capener, C.E., Proks, P., Ashcroft, F.M., Sansom, M.S.P., 2003. Filter Flexibility in a Mammalian K Channel: Models and Simulations of Kir6.2 Mutants. Biophys. J . 84 (4), 2345–2354.

Carr, J.K., Zabuga, A.V., Roy, S., Rizzo, T.R., Skinner, J.L., 2014. Assessment of amide I spectroscopic maps for a gas-phase peptide using IR-UV double-resonance spectroscopy and density functional theory calculations. J. Chem. Phys. 140 (22), 224111.

Chirlian, L.E., Francl, M.M., 1987. Atomic charges derived from electrostatic potentials: A detailed study. J. Comput. Chem. 8 (6), 894–905.

Chowdhary, J., Harder, E., Lopes, P.E., Huang, L., MacKerell Jr, A.D., Roux, B., 2013. A polarizable force field of dipalmitoylphosphatidylcholine based on the classical drude model for molecular dynamics simulations of lipids. J. Phys. Chem. B 117 (31), 9142–9160.

Chowdhary, J., Harder, E., Lopes, P.E.M., Huang, L., MacKerell Jr., A.D., Roux, B., 2013. A Polarizable Force Field of Dipalmitoylphosphatidylcholine Based on the Classical Drude Model for Molecular Dynamics Simulations of Lipids. J. Phys. Chem. B 117 (31), 9142–9160.

Compoint, M., Ramseyer, C., Huetz, P., 2004. Ab initio investigation of the atomic charges in the KcsA channel selectivity filter. Chem. Phys. Lett. 397 (4), 510–515.

Cordero-Morales, J.F., Cuello, L.G., Zhao, Y., Jogini, V., Cortes, D.M., Roux, B., Perozo, E., 2006. Molecular determinants of gating at the potassium-channel selectivity filter. Nat. Struct. Mol. Biol. 13 (4), 311–318.

Cuello, L.G., Jogini, V., Cortes, D.M., Perozo, E., 2010. Structural mechanism of C-type inactivation in K$^+$ channels. Nature 466 (7303), 203–208.

Cuello, L.G., Cortes, D.M., Perozo, E., 2017. The gating cycle of a K$^+$ channel at atomic resolution. Elife 6, e28032.

Cunha, A.V., Bondarenko, A.S., Jansen, T.L.C., 2016. Assessing Spectral Simulation Protocols for the Amide I Band of Proteins. J. Chem. Theory Comput. 12 (8), 3982–3992.

Demo, S.D., Yellen, G., 1992. Ion effects on gating of the Ca^{2+}-activated K$^+$ channel correlate with occupancy of the pore. Biophys. J. 61 (3), 639–648.

Domene, C., Furini, S., 2009. Dynamics, Energetics, and Selectivity of the Low-K$^+$ KcsA Channel Structure. J. Mol. Biol. 389 (3), 637–645.

Domene, C., Sansom, M.S.P., 2003. Potassium Channel, Ions, and Water: Simulation Studies Based on the High Resolution X-Ray Structure of KcsA. Biophys. J. 85 (5), 2787–2800.

Domene, C., Ocello, R., Masetti, M., Furini, S., 2021. Ion Conduction Mechanism as a Fingerprint of Potassium Channels. J. Am. Chem. Soc. 143 (31), 12181–12193.

Doyle, D.A., Cabral, J.M., Pfuetzner, R.A., Kuo, A., Gulbis, J.M., Cohen, S.L., Chait, B.T., MacKinnon, R., 1998. The Structure of the Potassium Channel: Molecular Basis of K$^+$ Conduction and Selectivity. Science 280 (5360), 69–77.

Eichmann, C.D., Frey, L., Maslennikov, I., Riek, R., 2019. Probing ion binding in the selectivity filter of the KcsA potassium channel. J. Am. Chem. Soc. 141 (18), 7391–7398.

Fowler, P.W., Tai, K., Sansom, M.S.P., 2008. The Selectivity of K$^+$ Ion Channels: Testing the Hypotheses. Biophys. J. 95 (11), 5062–5072.

Fowler, P.W., Abad, E., Beckstein, O., Sansom, M.S.P., 2013. Energetics of Multi-Ion Conduction Pathways in Potassium Ion Channels. J. Chem. Theory Comput. 9 (11), 5176–5189.

Furini, S., Domene, C., 2009. Atypical mechanism of conduction in potassium channels. Proc. Natl. Acad. Sci. U. S. A. 106 (38), 16074–16077.

Furini, S., Domene, C., 2020. Critical Assessment of Common Force Fields for Molecular Dynamics Simulations of Potassium Channels. J. Chem. Theory Comput. 16 (11), 7148–7159.

Ghosh, A., Ostrander, J.S., Zanni, M.T., 2017. Watching Proteins Wiggle: Mapping Structures with Two-Dimensional Infrared Spectroscopy. Chem. Rev. 117 (16), 10726–10759.

Gibor, G., Yakubovich, D., Rosenhouse-Dantsker, A., Peretz, A., Schottelndreier, H., Seebohm, G., Dascal, N., Logothetis, D.E., Paas, Y., Attali, B., 2007. An Inactivation Gate in the Selectivity Filter of KCNQ1 Potassium Channels. Biophys. J. 93 (12), 4159–4172.

Guidoni, L., Carloni, P., 2002. Potassium permeation through the KcsA channel: a density functional study. Biochim. Biophys. Acta Biomembr. 1563 (1), 1–6.

Guidoni, L., Torre, V., Carloni, P., 2000. Water and potassium dynamics inside the KcsA K$^+$ channel. FEBS Lett. 477 (1–2), 37–42.

Hamm, P., Zanni, M., 2011. Concepts and Methods of 2D Infrared Spectroscopy. Cambridge University Press, New York.

Heer, F.T., Posson, D.J., Wojtas-Niziurski, W., Nimigean, C.M., Bernèche, S., 2017. Mechanism of activation at the selectivity filter of the KcsA K$^+$ channel. Elife 6, e25844.

Hinsen, K., Roux, B., 1997. A potential function for computer simulation studies of proton transfer in acetylacetone. J. Comput. Chem. 18 (3), 368–380.

Hodgkin, A.L., Keynes, R., 1955. The potassium permeability of a giant nerve fibre. J. Physiol. 128 (1), 61.

Huetz, P., Boiteux, C., Compoint, M., Ramseyer, C., Girardet, C., 2006. Incidence of partial charges on ion selectivity in potassium channels. J. Chem. Phys. 124 (4), 044703.

Iwamoto, M., Oiki, S., 2011. Counting ion and water molecules in a streaming file through the open-filter structure of the K channel. J. Neurosci. 31 (34), 12180–12188.

Jensen, M.Ø., Jogini, V., Eastwood, M.P., Shaw, D.E., 2013. Atomic-level simulation of current–voltage relationships in single-file ion channels. J. Gen. Physiol. 141 (5), 619–632.

Jing, Z., Liu, C., Cheng, S.Y., Qi, R., Walker, B.D., Piquemal, J.-P., Ren, P., 2019. Polarizable Force Fields for Biomolecular Simulations: Recent Advances and Applications. Annu. Rev. Biophys. 48 (1), 371–394.

Khalili-Araghi, F., Tajkhorshid, E., Schulten, K., 2006. Dynamics of K$^+$ ion conduction through Kv1. 2. Biophys. J. 91 (6), L72–L74.

Klesse, G., Rao, S., Tucker, S.J., Sansom, M.S.P., 2020. Induced Polarization in Molecular Dynamics Simulations of the 5-HT3 Receptor Channel. J. Am. Chem. Soc. 142 (20), 9415–9427.

Kopec, W., Köpfer, D.A., Vickery, O.N., Bondarenko, A.S., Jansen, T.L., De Groot, B.L., Zachariae, U., 2018. Direct knock-on of desolvated ions governs strict ion selectivity in K$^+$ channels. Nat. Chem. 10 (8), 813–820.

Kopec, W., Rothberg, B.S., de Groot, B.L., 2019. Molecular mechanism of a potassium channel gating through activation gate-selectivity filter coupling. Nat. Commun. 10 (1), 5366.

Köpfer, D.A., Song, C., Gruene, T., Sheldrick, G.M., Zachariae, U., de Groot, B.L., 2014. Ion permeation in K+ channels occurs by direct Coulomb knock-on. Science 346 (6207), 352–355.

Kraszewski, S., Boiteux, C., Ramseyer, C., Girardet, C., 2009. Determination of the charge profile in the KcsA selectivity filter using ab initio calculations and molecular dynamics simulations. Phys. Chem. Chem. Phys. 11 (38), 8606–8613.

Kratochvil, H.T., Carr, J.K., Matulef, K., Annen, A.W., Li, H., Maj, M., Ostmeyer, J., Serrano, A.L., Raghuraman, H., Moran, S.D., et al., 2016. Instantaneous ion configurations in the K$^+$ ion channel selectivity filter revealed by 2D IR spectroscopy. Science 353 (6303), 1040–1044.

Kwak, K., Park, S., Finkelstein, I.J., Fayer, M.D., 2007. Frequency-frequency correlation functions and apodization in two-dimensional infrared vibrational echo spectroscopy: A new approach. J. Chem. Phys. 127 (12), 124503.

Kwak, K., Rosenfeld, D.E., Fayer, M.D., 2008. Taking apart the two-dimensional infrared vibrational echo spectra: More information and elimination of distortions. J. Chem. Phys. 128 (20), 204505.

la Cour Jansen, T., Dijkstra, A.G., Watson, T.M., Hirst, J.D., Knoester, J., 2006. Modeling the amide I bands of small peptides. J. Chem. Phys. 125 (4), 044312.

Lam, C.K., de Groot, B.L., 2023. Ion Conduction Mechanisms in Potassium Channels Revealed by Permeation Cycles. J. Chem. Theory Comput 19 (9), 2574–2589.

Lamoureux, G., Harder, E., Vorobyov, I.V., Roux, B., MacKerell, A.D., 2006. A polarizable model of water for molecular dynamics simulations of biomolecules. Chem. Phys. Lett. 418 (1), 245–249.

Langan, P.S., Vandavasi, V.G., Weiss, K.L., Afonine, P.V., El Omari, K., Duman, R., Wagner, A., Coates, L., 2018. Anomalous X-ray diffraction studies of ion transport in K$^+$ channels. Nat. Commun. 9 (1), 4540.

LeMasurier, M., Heginbotham, L., Miller, C., 2001. Kcsa: It's a Potassium Channel. J. Gen. Physiol. 118 (3), 303–314.

Li, H., Ngo, V., Da Silva, M.C., Salahub, D.R., Callahan, K., Roux, B., Noskov, S.Y., 2015. Representation of Ion-Protein Interactions Using the Drude Polarizable Force-Field. J. Phys. Chem. B 119 (29), 9401–9416.

Li, J., Ostmeyer, J., Cuello, L.G., Perozo, E., Roux, B., 2018. Rapid constriction of the selectivity filter underlies C-type inactivation in the KcsA potassium channel. J. Gen. Physiol. 150 (10), 1408–1420.

Liang, C., Jansen, T.L., 2012. An efficient N3-scaling propagation scheme for simulating two-dimensional infrared and visible spectra. J. Chem. Theory Comput. 8 (5), 1706–1713.

Littleton, J.T., Ganetzky, B., 2000. Ion channels and synaptic organization: analysis of the drosophila genome. Neuron 26 (1), 35–43.

Lopes, P.E.M., Huang, J., Shim, J., Luo, Y., Li, H., Roux, B., MacKerell Jr., A.D., 2013. Polarizable Force Field for Peptides and Proteins Based on the Classical Drude Oscillator. J. Chem. Theory Comput. 9 (12), 5430–5449.

Lopes, P.E., Huang, J., Shim, J., Luo, Y., Li, H., Roux, B., MacKerell Jr, A.D., 2013. Polarizable force field for peptides and proteins based on the classical drude oscillator. J. Chem. Theory Comput. 9 (12), 5430–5449.

MacKinnon, R., Cohen, S.L., Kuo, A., Lee, A., Chait, B.T., 1998. Structural Conservation in Prokaryotic and Eukaryotic Potassium Channels. Science 280 (5360), 106–109.

Mendez-Otalvaro, E., Kopec, W., de Groot, B.L., 2004. Effect of two activators on the gating of a K$_{2P}$ channel, 2019 bioRxiv 2024 (2024).

Morais-Cabral, J.H., Zhou, Y., MacKinnon, R., 2001. Energetic optimization of ion conduction rate by the K$^+$ selectivity filter. Nature 414 (6859), 37–42.

Mukherjee, P., Krummel, A.T., Fulmer, E.C., Kass, I, Arkin, I.T., Zanni, M.T., 2004. Site-specific vibrational dynamics of the CD3ζ membrane peptide using heterodyned two-dimensional infrared photon echo spectroscopy. J. Chem. Phys. 120 (21), 10215–10224.

Mukherjee, P., Kass, I., Arkin, I.T., Zanni, M.T., 2006. Picosecond dynamics of a membrane protein revealed by 2D IR. Proc. Natl. Acad. Sci. U. S. A. 103 (10), 3528–3533.

Noskov, S.Y., Roux, B., 2006. Ion selectivity in potassium channels. Biophys. Chem. 124 (3), 279–291.

Oostenbrink, C., Villa, A., Mark, A.E., Van Gunsteren, W.F., 2004. A biomolecular force field based on the free enthalpy of hydration and solvation: The GROMOS force-field parameter sets 53A5 and 53A6. J. Comput. Chem. 25 (13), 1656–1676.

Öster, C., Hendriks, K., Kopec, W., Chevelkov, V., Shi, C., Michl, D., Lange, S., Sun, H., de Groot, B.L., Lange, A., 2019. The conduction pathway of potassium channels is water free under physiological conditions. Sci. Adv. 5 (7) eaaw6756.

Petersen, H.G., 1995. Accuracy and efficiency of the particle mesh Ewald method. J. Chem. Phys. 103 (9), 3668–3679.

Petti, M.K., Lomont, J.P., Maj, M., Zanni, M.T., 2018. Two-Dimensional Spectroscopy Is Being Used to Address Core Scientific Questions in Biology and Materials Science. J. Phys. Chem. B 122 (6), 1771–1780.

Phillips, J.C., Braun, R., Wang, W., Gumbart, J., Tajkhorshid, E., Villa, E., Chipot, C., Skeel, R.D., Kalé, L., Schulten, K., 2005. Scalable molecular dynamics with NAMD. J. Comput. Chem. 26 (16), 1781–1802.

Rauh, O., Hansen, U., Scheub, D., Thiel, G., Schroeder, I., 2018. Site-specific ion occupation in the selectivity filter causes voltage-dependent gating in a viral K+ channel. Sci. Rep. 8 (1), 10406.

Reppert, M., Tokmakoff, A., 2016. Computational Amide I 2D IR Spectroscopy as a Probe of Protein Structure and Dynamics. Annu. Rev. Phys. Chem. 67, 359–386.

Ritchie, J.P., Bachrach, S.M., 1987. Some methods and applications of electron density distribution analysis. J. Comput. Chem. 8 (4), 499–509.

Ryan, M.J., Gao, L., Valiyaveetil, F.I., Zanni, M.T., Kananenka, A.A., 2023. Probing Ion Configurations in the KcsA Selectivity Filter with Single-Isotope Labels and 2D IR Spectroscopy. J. Am. Chem. Soc. 145 (33), 18529–18537.

Ryan, M.J., Gao, L., Valiyaveetil, F.I., Kananenka, A.A., Zanni, M.T., 2024. Water inside the Selectivity Filter of a K+ Ion Channel: Structural Heterogeneity, Picosecond Dynamics, and Hydrogen Bonding. J. Am. Chem. Soc. 146 (2), 1543–1553.

Schewe, M., Nematian-Ardestani, E., Sun, H., Musinszki, M., Cordeiro, S., Bucci, G., de Groot, B.L., Tucker, S.J., Rapedius, M., Baukrowitz, T., 2016. A non-canonical voltage-sensing mechanism controls gating in K2P K+ channels. Cell 164 (5), 937–949.

Scott, W.R.P., Hünenberger, P.H., Tironi, I.G., Mark, A.E., Billeter, S.R., Fennen, J., Torda, A.E., Huber, T., Krüger, P., van Gunsteren, W.F., 1999. The GROMOS Biomolecular Simulation Program Package. Chem. A Eur. J. 103 (19), 3596–3607.

Shrivastava, I.H., Sansom, M.S., 2000. Simulations of ion permeation through a potassium channel: molecular dynamics of KcsA in a phospholipid bilayer. Biophys. J. 78 (2), 557–570.

Singh, U.C., Kollman, P.A., 1984. An approach to computing electrostatic charges for molecules. J. Comput. Chem. 5 (2), 129–145.

Strong, S.E., Hestand, N.J., Kananenka, A.A., Zanni, M.T., Skinner, J.L., 2020. IR Spectroscopy Can Reveal the Mechanism of K(+) Transport in Ion Channels. Biophys. J. 118 (1), 254–261.

Swenson, R.P., Armstrong, C.M., 1981. K+ channels close more slowly in the presence of external K+ and Rb+. Nature 291 (5814), 427–429.

Tilegenova, C., Cortes, D.M., Jahovic, N., Hardy, E., Hariharan, P., Guan, L., Cuello, L.G., 2019. Structure, function, and ion-binding properties of a K+ channel stabilized in the 2, 4-ion–bound configuration. Proc. Natl. Acad. Sci. U. S. A. 116 (34), 16829–16834.

Torii, H., Tasumi, M., 1998. Ab initio molecular orbital study of the amide I vibrational interactions between the peptide groups in di-and tripeptides and considerations on the conformation of the extended helix. J. Raman Spectrosc. 29 (1), 81–86.

Valiyaveetil, F.I., Leonetti, M., Muir, T.W., MacKinnon, R., 2006. Ion Selectivity in a Semisynthetic K+ Channel Locked in the Conductive Conformation. Science 314 (5801), 1004–1007.

Van Der Spoel, D., Lindahl, E., Hess, B., Groenhof, G., Mark, A.E., Berendsen, H.J.C., 2005. GROMACS: Fast, flexible, and free. J. Comput. Chem. 26 (16), 1701–1718.

Wang, L., Middleton, C.T., Singh, S., Reddy, A.S., Woys, A.M., Strasfeld, D.B., Marek, P., Raleigh, D.P., De Pablo, J.J., Zanni, M.T., 2011. 2DIR spectroscopy of human amylin fibrils reflects stable β-sheet structure. J. Am. Chem. Soc. 133 (40), 16062–16071.

Wang, L., Middleton, C.T., Zanni, M.T., Skinner, J.L., 2011. Development and Validation of Transferable Amide I Vibrational Frequency Maps for Peptides. J. Phys. Chem. B 115 (13), 3713–3724.

Warshel, A., Kato, M., Pisliakov, A.V., 2007. Polarizable Force Fields: History, Test Cases, and Prospects. J. Chem. Theory Comput. 3 (6), 2034–2045.

Zhou, Y., MacKinnon, R., 2003. The Occupancy of Ions in the K+ Selectivity Filter: Charge Balance and Coupling of Ion Binding to a Protein Conformational Change Underlie High Conduction Rates. J. Mol. Biol. 333 (5), 965–975.

Zhou, Y., Morais-Cabral, J.H., Kaufman, A., MacKinnon, R., 2001. Chemistry of ion coordination and hydration revealed by a K+ channel–Fab complex at 2.0 Å resolution. Nature 414 (6859), 43–48.